face roughness and come close to the ones theoretically anticipated in Fig. 1. Their footprint is 40 by 40 μm.

Figure 4 compares measured and calculated optical transmittance spectra for circular polarization of the incoming light propagating along the helix axis. Broadband optical spectroscopy in the few-μm wavelength range using incident circular polarization of light is not standard at all. Thus, by introducing the combination of a linear polarizer and a mid-infrared super-achromatic quarter-wave plate, we have specifically modified a commercial Fourier-transform spectrometer combined with a microscope for that purpose (*18*). The measured spectra in Fig. 4 reveal the theoretically anticipated blocking of one of the two circular polarizations, whereas the other circular polarization is transmitted. A large transmittance ratio results in the wavelength range from 3.5 to 7.5 μm, which exceeds one octave. Some engineering of the helix parameters would allow for further improvement of the suppression ratio. For conical helices with a diameter that continuously increases along the helix axis—rather than for the constant helix diameter discussed here—antenna theory (*28*, *29*) promises bandwidths considerably exceeding one octave. This approach could lead to a further increase of the circular-polarizer operation bandwidth.

Metallic wire-grid linear polarizers ("one-dimensional metamaterials") have been known since the pioneering experiments on electromagnetic waves by Heinrich Hertz in 1887. Nowadays, they are still widely used for broadband applications. Because of the obvious wavelength dependence of quarter-wave plates, broadband conversion of linear into circular polarization is nontrivial in many frequency ranges. Our 3D metamaterial based on metal helices can be viewed as the circular analog of Hertz's device.

References and Notes

1. D. R. Smith, J. B. Pendry, M. C. K. Wiltshire, *Science* **305**, 788 (2004).
2. C. M. Soukoulis, S. Linden, M. Wegener, *Science* **315**, 47 (2007).
3. V. M. Shalaev, *Nat. Photon.* **1**, 41 (2006).
4. J. B. Pendry, *Phys. Rev. Lett.* **85**, 3966 (2000).
5. U. Leonhardt, *Science* **312**, 1777 (2006).
6. J. B. Pendry, D. Schurig, D. R. Smith, *Science* **312**, 1780 (2006).
7. D. Schurig *et al.*, *Science* **314**, 977 (2006).
8. J. B. Pendry, *Science* **306**, 1353 (2004).
9. A. V. Rogacheva, V. A. Fedotov, A. S. Schwanecke, N. I. Zheludev, *Phys. Rev. Lett.* **97**, 177401 (2006).
10. M. Decker, M. W. Klein, M. Wegener, S. Linden, *Opt. Lett.* **32**, 856 (2007).
11. E. Plum *et al.*, *Phys. Rev. B* **79**, 035407 (2009).
12. S. Zhang *et al.*, *Phys. Rev. Lett.* **102**, 023901 (2009).
13. M. Wegener, S. Linden, *Physics* **2**, 3 (2009).
14. E. Hecht, *Optics* (Addison-Wesley, San Francisco, ed. 4, 2002), chap. 8.
15. M. S. Rill *et al.*, *Nat. Mater.* **7**, 543 (2008).
16. N. Liu, H. Liu, S. Zhu, H. Giessen, *Nat. Photon.* **3**, 157 (2009).
17. M. G. Silveirinha, *IEEE Trans. Antenn. Propag.* **56**, 390 (2008).
18. Materials and methods are available as supporting material on *Science* Online.
19. J. B. Pendry, A. J. Holden, D. J. Robbins, W. J. Steward, *IEEE Trans. Microw. Theory Tech.* **47**, 2075 (1999).
20. S. Linden *et al.*, *Science* **306**, 1351 (2004).
21. R. Abdeddaïm, G. Guida, A. Priou, B. Gallas, J. Rivory, *Appl. Phys. Lett.* **94**, 081907 (2009).
22. E. Plum, V. A. Fedotov, N. I. Zheludev, *Appl. Phys. Lett.* **93**, 191911 (2008).
23. E. Plum *et al.*, *Phys. Rev. Lett.* **102**, 113902 (2009).
24. C. Enkrich *et al.*, *Phys. Rev. Lett.* **95**, 203901 (2005).
25. E. Shamonina, L. Solymar, *J. Magn. Magn. Mater.* **300**, 38 (2006).
26. K. Busch *et al.*, *Phys. Rep.* **444**, 101 (2007).
27. W. Zhou *et al.*, *Science* **296**, 1106 (2002).
28. J. S. Chatterjee, *J. Appl. Phys.* **24**, 550 (1953).
29. J. D. Dyson, *IRE Trans. Antennas Propag.* **7**, 181 (1959).

30. We thank I. Staude for help regarding the optical measurements and C. E. Kriegler for discussions. We acknowledge support by the Deutsche Forschungsgemeinschaft (DFG) and the State of Baden-Württemberg through the DFG Center for Functional Nanostructures (CFN) within subprojects A1.4 and A1.5. The project PHOME acknowledges the financial support of the Future and Emerging Technologies (FET) program within the Seventh Framework Programme for Research of the European Commission, under FET Open grant 213390. The project METAMAT is supported by the Bundesministerium für Bildung und Forschung (BMBF). The research of S.L. is further supported through a Helmholtz-Hochschul-Nachwuchsgruppe (VH-NG-232) and that of G.v.F. through a DFG Emmy-Noether fellowship (DFG-Fr 1671/4-3). The Ph.D. education of J.K.G., M.T., M.S.R., and M.D. is embedded in the Karlsruhe School of Optics and Photonics (KSOP).

Supporting Online Material

www.sciencemag.org/cgi/content/full/1177031/DC1
Materials and Methods

29 May 2009; accepted 4 August 2009
Published online 20 August 2009;
10.1126/science.1177031
Include this information when citing this paper.

Control of Spin Precession in a Spin-Injected Field Effect Transistor

Hyun Cheol Koo,[1] Jae Hyun Kwon,[1] Jonghwa Eom,[1,2] Joonyeon Chang,[1]* Suk Hee Han,[1] Mark Johnson[3]

Spintronics increases the functionality of information processing while seeking to overcome some of the limitations of conventional electronics. The spin-injected field effect transistor, a lateral semiconducting channel with two ferromagnetic electrodes, lies at the foundation of spintronics research. We demonstrated a spin-injected field effect transistor in a high-mobility InAs heterostructure with empirically calibrated electrical injection and detection of ballistic spin-polarized electrons. We observed and fit to theory an oscillatory channel conductance as a function of monotonically increasing gate voltage.

Many types of spintronic devices have been proposed, investigated, and developed. However, the spin-injected field effect transistor (spin FET), which lies at the heart of spintronics, has yet to be realized. Proposed by Datta and Das (*1*), the demonstration of a spin FET involves spin injection and detection using a ferromagnetic source and drain. However, a special feature of the spin FET is the periodic modulation of source-drain conductance as controlled by gate voltage–induced precession of the injected spins. Electrical spin injection and detection have been demonstrated in a variety of semiconductors (*2*–*6*). Carrier spin precession has been induced by using an external magnetic field and detecting the Hanle effect, a Lorentzian-shaped magnetoresistance caused by precessional dephasing of diffusing spins, in materials with relatively small spin-orbit interaction such as GaAs and Si (*3*–*5*). However, modulating the channel conductance by using an electric field to induce spin precession has remained elusive. A material with large spin-orbit interaction will not permit the observation of the Hanle effect, yet this type of material is necessary for gate voltage–induced spin precession. These two phenomena are mutually exclusive within any single material. We used a high-mobility InAs heterostructure with strong intrinsic spin-orbit interaction α, and we measured the nonlocal channel conductance (*5*, *6*) rather than the direct source-drain conductance suggested by Datta and Das. Conventional lateral spin valve techniques measured the population of ballistic spins. Shubnikov–de Haas (SdH) experiments provided an independent measurement of the dependence of the spin-orbit interaction on gate voltage. Apart from a small phase shift, the oscillatory conductance that we measured fits to theory (*1*) with no adjustable parameters. The temperature dependence indicates that the modulation is only observed when the injected electrons have ballistic trajectories to the detector.

A conventional lateral spin valve device (Fig. 1A) is a convenient structure to investigate spin injection and detection for several reasons. First, the ferromagnetic (FM) electrodes have a uniaxial shape anisotropy that can create binary

[1]Center for Spintronics Research, Korea Institute of Science and Technology (KIST), 39-1 Hawolgok-dong, Seongbuk-gu, Seoul, 136-791, Korea. [2]Department of Physics, Sejong University, 98 Gunja-dong, Gwangjin-gu, Seoul, 143-747, Korea. [3]Naval Research Laboratory, 4555 Overlook Avenue SW, Washington, DC 20375, USA.

*To whom correspondence should be addressed. E-mail: presto@kist.re.kr

magnetization states along the y axis, $\pm M_y$. A small external magnetic field applied along the y axis (B_a) can create conditions with the injector (source) and detector (drain) magnetizations parallel or antiparallel, resulting in relatively high or low spin-dependent voltages at the detector (*2*, *7*, *8*). Second, a small channel length, L, between injector and detector can be defined lithographically. Third, in the "nonlocal" configuration (*5*–*12*), the bias current is grounded at one end of the sample, there is no charge current in the vicinity of the spin detector, background effects are minimized, and the signal-to-noise ratio is maximized. Spin-polarized carriers with ballistic trajectories along the $+x$ and $-x$ directions are injected with equal probability.

In a two-dimensional electron gas (2DEG) channel with strong spin-orbit interaction, the structural asymmetry provides an intrinsic electric field along the z axis, $E_{z,0}$, where the subscripts denote the z direction and zero gate voltage. In the rest frame of a carrier moving with a weakly relativistic Fermi velocity, $v_{Fx} \sim c/300$, with c the speed of light, electric field $E_{z,0}$ transforms as an effective magnetic field $B_{Ry,0}$, which is called the Rashba field (*13*). The Rashba field is perpendicular to the directions of the carrier velocity and the electric field. In Fig. 1, $B_{Ry,0}$ is along the y axis and has no effect on carriers that are injected with spin polarization also along the y axis (Fig. 1A). Datta and Das predicted, however, that carriers injected with spin polarization along the x axis would precess under the influence of $B_{Ry,0}$, a condition that occurs when the magnetization of the injector is oriented along the x axis (Fig. 1B). The magnitude of E_z can be modulated by a variable gate voltage V_G, the magnitude of the Rashba field changes, B_{Ry} is proportional to E_z, and the precession rate therefore changes as a function of V_G. When the detector is also a FM electrode with magnetization along the x axis and carriers have ballistic trajectories from injector to detector, the channel conductance of the structure in Fig. 1B is predicted to oscillate periodically as a function of monotonically increasing gate voltage, because the detector voltage will be high when a detected spin has its orientation parallel with that of the detector and the detector voltage will be low when the spin is antiparallel (*1*). This is a relativistic electric field analog of Larmor waves (*14*). Whereas Larmor waves may be detected in superposition with a diffusive resonance feature, the spin-orbit interaction in a spin FET is so large that spin orientation is randomized after only a few scattering events, and the diffusive analog (the Hanle effect) is not observed [supporting online material (SOM) text S1].

Our devices consist of two $Ni_{81}Fe_{19}$ electrodes on top of an InAs high–electron mobility transistor (HEMT) channel and a gate electrode (*15*). The InAs HEMT (*6*, *16*) was grown by molecular beam epitaxy on a semi-insulating InP (100) substrate. The single quantum well, which functions as a 2DEG channel, has a depth of 35.5 nm from the top surface. The carrier density and mobility of the 2DEG are $n_S = 1.8 \times 10^{12}$ to 2.8×10^{12} cm^{-2} and $\mu = 50{,}000$ to $60{,}000$ cm^2 V^{-1} s^{-1} at temperature $T = 1.8$ K, respectively. The channel, defined by a mesa etch, is oriented with x along the <110> direction and has a width $w = 8$ μm. The two FM electrodes were fabricated with electron beam lithography and lift-off and have lateral dimensions of 0.4×80 μm and 0.5×40 μm (Fig. 1C). Samples were made with FM electrode spacings of $L = 1.25$ and 1.65 μm, measured center to center.

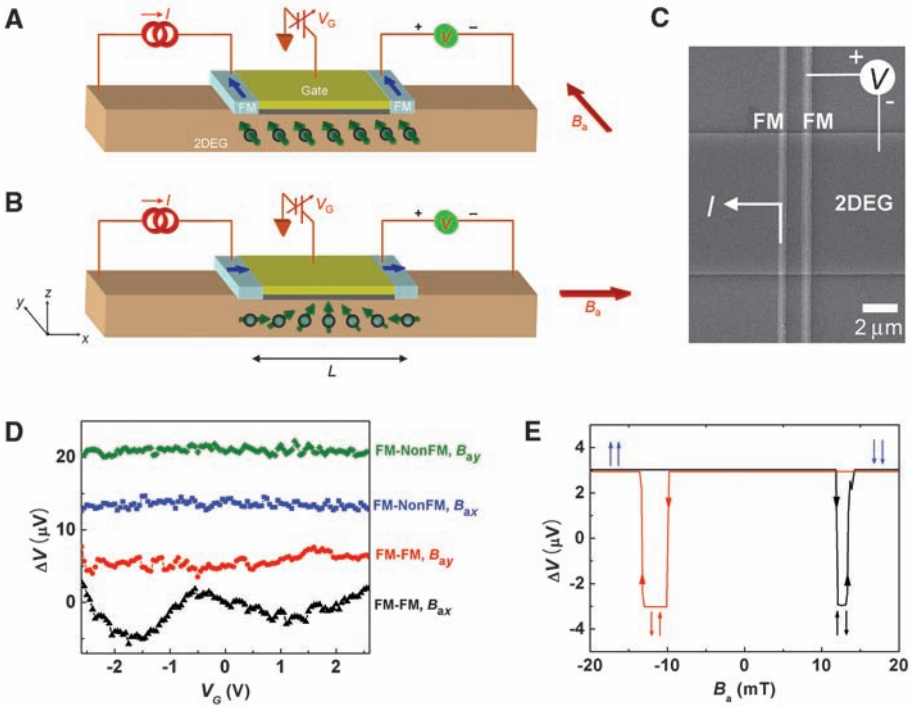

Fig. 1. Lateral gated spin valve device with an external magnetic field ($B_a = 0.5$ T) applied along the y axis (**A**) and x axis (**B**). In (A), the magnetizations of the FM electrodes are shown oriented along the y axis. The injected spin-polarized electrons are oriented along the y axis and do not precess under the influence of the Rashba field B_{Ry}. (B) shows the electrons injected with spin orientation along the x axis, perpendicular to B_{Ry}, and they precess under the influence of the effective field. (**C**) Scanning electron micrograph of the device. For clarity, the image was taken before depositing the gate oxide and electrode. (**D**) Observation of oscillatory conductance from injector to detector with $T = 1.8$ K. Gate-controlled spin precession occurs in configuration (B) (black trace) and not in configuration (A) (red trace). The green and blue traces represent data from a control sample that has a ferromagnetic injector but a nonmagnetic detector. The channel length is $L = 1.65$ μm and the bias current is $I = 1$ mA. The plots are shifted for clarity. (**E**) Conventional, nonlocal, lateral spin valve magnetoresistance measurement using configuration (A) at $T = 1.8$ K. The black and red lines correspond to field sweep-up and -down, respectively. The pairs of arrows indicate the magnetization alignments of the two FM electrodes, either parallel or antiparallel.

An example of the oscillatory conductance modulation is shown in Fig. 1D. An external magnetic field, $B_a = 0.5$ T, was applied to fix the magnetization orientations of the FM electrodes in a chosen direction, thereby determining the axis of spin injection and detection. The nonlocal channel conductance was measured as a function of gate voltage for the range $-3 \le V_G \le 3$ V. The red trace presents data for field B_{ay} applied along the y axis (Fig. 1A). The orientation of injected spins along the y axis is parallel to the Rashba field. There was no spin precession and no modulation of voltage recorded by the detector. For the data represented by the black trace, the external field $B_{ax} = 0.5$ T was large enough to overcome the shape anisotropy of the FM electrodes. The magnetization orientations of injector and detector are along the $+x$ direction (Fig. 1B), and the injected spin orientation is perpendicular to the Rashba field. The spin precession varies as a function of gate voltage, and an oscillation of detected voltage as a function of V_G was observed. The range of gate voltage is sufficiently large that more than one full cycle of voltage oscillation was recorded.

Control experiments were performed to further confirm that the voltage oscillation originated from the detection of spin precession in the channel. The devices used as controls were made with the same geometry and lithographic processing but with the FM detector replaced by a nonmagnetic electrode composed of an In (50 nm)/Au (30 nm) film. Identical transport measurements were made, but no voltage modulation was observed, regardless of the direction of the external field (blue and green traces in Fig. 1D).

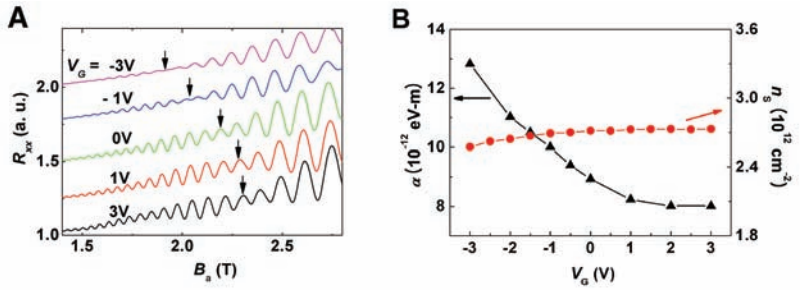

Fig. 2. Gate control of spin-orbit interaction at T = 1.8 K. (**A**) SdH oscillations as a function of gate voltage. The channel resistance R_{xx} is measured with a magnetic field, B_a, that is perpendicular to the 2DEG plane. (**B**) Spin-orbit interaction parameter α, deduced from (A), and carrier concentration n_S, as functions of gate voltage. Because of the asymmetry of the quantum well structure, α is nonzero at V_G = 0.

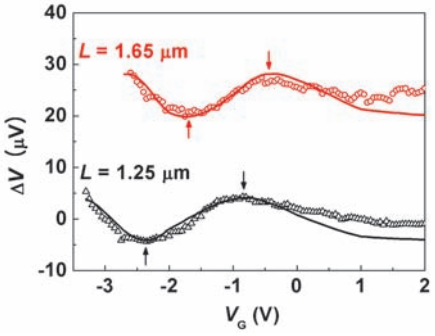

Fig. 3. Gate voltage modulation of spin FETs having different channel lengths, with T = 1.8 K and I = 1 mA. The symbols indicate experimental data. The solid lines are the fits obtained from Eq. 1. Data are offset for clarity. Baseline voltages are 1.032 mV and 0.715 mV for L = 1.25 μm and 1.65 μm, respectively.

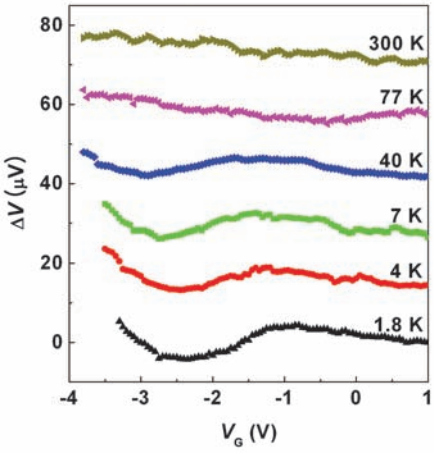

Fig. 4. Temperature dependence of oscillatory conductance with L = 1.25 μm and I = 1 mA. As temperature increases, the mean free path decreases and transport characteristics change from ballistic to diffusive.

A set of experiments was performed to enable quantitative analysis and detailed comparison with theory. Data from a conventional lateral spin valve measurement (*5*, *6*, *8*–*12*) are shown in Fig. 1E. In the absence of an external magnetic field, the magnetizations of the injector and detector have bistable states along the ±y axis because of their shape anisotropy, and they have slightly different coercivities because of the different aspect ratios. With V_G = 0 and constant bias current I = 1 mA, a small magnetic field was swept along the y axis, the magnetization alignment of FM electrodes changed between parallel and antiparallel configurations, and the detector voltage V was high or low, respectively. The characteristic dips seen in the data were observed for $B_a > 0$, when the field sweep was from negative to positive (black trace), and for $B_a < 0$, when the field sweep was from positive to negative (red trace). The spacing L between the injector and the detector is less than a carrier mean free path, l, and measurements are dominated by ballistic transport effects. There is no formal theory for the magnitude of the lateral spin valve effect for ballistic carriers. Instead, this conventional lateral spin valve measurement provides a calibration for the amplitude of the voltage oscillation in Fig. 1D, because the mechanism for spin-dependent voltage is the same for both experiments. The magnitude of the dips, $A \equiv \Delta V = 6 \pm 0.2$ μV, is the same as the amplitude of the oscillatory voltage shown in Fig. 1D, $\Delta V = 6 \pm 0.5$ μV, and this empirically measured amplitude A was used for the quantitative fits.

Next, the spin-orbit coupling strength α was measured as a function of gate voltage. SdH oscillations (*17*, *18*) were measured at a variety of gate voltage values, beat patterns were observed (Fig. 2A), and $\alpha(V_G)$ was deduced (SOM text S2). The changing nodal position of the beat pattern (arrows in Fig. 2A) shows that the gate voltage strongly affects the spin-orbit coupling of carriers in the InAs single-quantum well. The magnitude of $\alpha(V_G)$ is strongly dependent on V_G for the range $-3 \le V_G \le 1$ V (Fig. 2B). The effect of the gate voltage is enhanced for the negative V_G because of nonlinear bending of the quantum well. The dependence of α on V_G is weak for the positive range $1 \le V_G \le 3$ V. Although magneto-intersubband scattering may also cause an oscillatory magnetoresistance (*19*, *20*), this mechanism can be excluded from an interpretation of our data by using a detailed analysis of the Fourier transforms of the SdH oscillations (SOM text S3). Because the gate voltage might be expected to change the carrier concentration in the channel, the voltage-dependent concentration $n(V_G)$ was directly determined from Hall measurements. It shows negligible variation over the experimental range of V_G (Fig. 2B). Having measured $\alpha(V_G)$, the magnitude of the Rashba field is readily calculated from $B_{Ry} = 2\alpha k_F/(g\mu_B)$ (*1*), where k_F and g are the Fermi wave vector and g factor, respectively, of the carriers in the channel, and $\mu_B = 9.27 \times 10^{-24}$ J/T is the Bohr magneton. Using $k_F = 4.13 \times 10^6$ cm^{-1} and $g = 15$ (*21*), the field at zero gate voltage (Fig. 2B) has magnitude $B_{Ry} = 8.5$ T. $B_a = 0.5$ T is an order of magnitude smaller than B_R and has a negligible effect on spin precession.

The theory of Datta and Das describes the transport of ballistic electrons in a 2DEG channel (SOM text S4). Allowing for an arbitrary phase shift φ, the expression for the detector voltage is

$$V = A\cos(2m^*\alpha L/\hbar^2 + \varphi) \qquad (1)$$

The fit for the sample with L = 1.65 μm and $m^* = 0.05m_0$ (*22*),where m_0 is 9.1×10^{-31} kg and $\hbar$ is Planck's constant divided by 2π, using the empirical values of $\alpha(V_G)$ and A, is plotted in Fig. 3 as a solid line and shows excellent quantitative agreement with the data. The phase shift φ, believed to be a consequence of shielding near the metallic ferromagnetic electrodes, is the only adjustable fitting parameter. The data fit well for more than a full wavelength of oscillation, with a small weakness of the fit occurring for the regime where gate voltage modulation of α is weak, $V_G > 0$ V.

Because precessional phase accumulation is proportional to L, it follows that carriers in a device with shorter spacing L will require a larger range of α, and therefore a larger range of gate voltage V_G to precess by π radians. A sample with L = 1.25 μm was fabricated and the data and fit are shown as the bottom trace in Fig. 3. The half period of oscillation is seen to increase from ΔV_G = 1.24 V (L = 1.65 μm) to ΔV_G = 1.53 V (L = 1.25 μm). Data with different values of L are fit successfully by Eq. 1 with no adjustable parameter other than a small phase shift.

The temperature dependence of the oscillatory voltage is shown in Fig. 4. Gate voltage modulation is clearly observed up to T = 40 K. From the Dyakonov-Kachorovski (*23*) and Dyakonov-Perel (*24*) mechanisms, the spin relaxation rate $1/\tau_s$ scales as $TE_1^2\tau_p$ in a narrow quantum well such as ours. Here E_1 is the confinement energy of the quantum well and τ_p is the momentum scattering time. In our experiments, τ_p is nearly proportional to $1/T$, and therefore the additional spin relaxation at higher temperature is negligible (*6*). At high temperatures, however, inelastic scat-

tering becomes more pronounced. Our measurements of the temperature dependence of the mean free path (SOM text S5) show that the conductance oscillation broadens and disappears in the same temperature range ($T \geq 40$ K) where l becomes shorter and transport therefore changes from ballistic to diffusive. This temperature dependence is a further confirmation of theory (*1*).

Two decades ago, Datta and Das proposed an experiment involving spin injection, detection, and spin precession caused by a gate voltage and special relativistic effects on ballistic electrons in a 2DEG. Separate aspects have been demonstrated individually (*3*, *5*, *17*). We have used the nonlocal lateral spin valve geometry to combine these aspects in a single experiment. The InAs single-quantum well used here is an ideal material, because a large spin-orbit interaction modulates a Rashba field by several teslas with a gate voltage range of a few volts.

References and Notes

1. S. Datta, B. Das, *Appl. Phys. Lett.* **56**, 665 (1990).
2. I. Žutić, J. Fabian, S. Das Sarma, *Rev. Mod. Phys.* **76**, 323 (2004).
3. S. A. Crooker *et al.*, *Science* **309**, 2191 (2005).
4. I. Appelbaum, B. Huang, D. J. Monsma, *Nature* **447**, 295 (2007).
5. X. Lou *et al.*, *Nat. Phys.* **3**, 197 (2007).
6. H. C. Koo *et al.*, *Appl. Phys. Lett.* **90**, 022101 (2007).
7. M. Johnson, *Science* **260**, 320 (1993).
8. M. Johnson, R. H. Silsbee, *Phys. Rev. Lett.* **55**, 1790 (1985).
9. F. J. Jedema, H. B. Heersche, A. T. Filip, J. J. A. Baselmans, B. J. van Wees, *Nature* **416**, 713 (2002).
10. Y. Ji, A. Hoffmann, J. S. Jiang, S. D. Bader, *Appl. Phys. Lett.* **85**, 6218 (2004).
11. T. Kimura, J. Hamrle, Y. Otani, K. Tsukagoshi, A. Aoyagi, *Appl. Phys. Lett.* **85**, 3501 (2004).
12. M. Johnson, R. H. Silsbee, *Phys. Rev. B* **76**, 153107 (2007).
13. Yu. A. Bychkov, E. I. Rashba, *JETP Lett.* **39**, 78 (1984).
14. A. Janossy, P. Monod, *Phys. Rev. Lett.* **37**, 612 (1976).
15. Materials and methods are available as supporting material on *Science* Online.
16. J. Nitta, A. Tatsushi, H. Takayanagi, T. Enoki, *Physica E* **2**, 527 (1998).
17. J. Nitta, T. Akazaki, H. Takayanagi, T. Enoki, *Phys. Rev. Lett.* **78**, 1335 (1997).
18. I. Lo *et al.*, *Phys. Rev. B* **65**, 161306(R) (2002).
19. T. H. Sander, S. N. Holmes, J. J. Harris, D. K. Maude, J. C. Portal, *Phys. Rev. B* **58**, 13856 (1998).
20. A. C. H. Rowe, J. Nehls, R. A. Stradling, R. S. Ferguson, *Phys. Rev. B* **63**, 201307 (2001).
21. V. Ya. Aleshkin *et al.*, *Semiconductors* **42**, 828 (2008).
22. C.-M. Hu, J. Nitta, A. Jensen, J. B. Hansen, H. Takayanagi, *Phys. Rev. B* **63**, 125333 (2001).
23. M. I. D'yakonov, V. Yu. Kachorovski. *Fiz. Tekh. Poluprodn.* **20**, 178 (1986) [*Sov. Phys. Semicond.* **20**, 110 (1986)].
24. M. I. D'yakonov, V. I. Perel. *Fiz. Tverd. Tela* **13**, 3581 (1971) [*Sov. Phys. Solid State* **13**, 3023 (1972)].

25. This work was supported by the Korea Institute of Science and Technology Institutional Program.

Supporting Online Material

www.sciencemag.org/cgi/content/full/325/5947/1515/DC1
Materials and Methods
SOM Text
Figs. S1 to S5
References

17 March 2009; accepted 28 July 2009
10.1126/science.1173667

Memory Metamaterials

T. Driscoll,[1]* Hyun-Tak Kim,[2] Byung-Gyu Chae,[2] Bong-Jun Kim,[2] Yong-Wook Lee,[2,3] N. Marie Jokerst,[4] S. Palit,[4] D. R. Smith,[4] M. Di Ventra,[1] D. N. Basov[1]

The resonant elements that grant metamaterials their distinct properties have the fundamental limitation of restricting their useable frequency bandwidth. The development of frequency-agile metamaterials has helped to alleviate these bandwidth restrictions by allowing real-time tuning of the metamaterial frequency response. We demonstrate electrically controlled persistent frequency tuning of a metamaterial, which allows the lasting modification of its response by using a transient stimulus. This work demonstrates a form of memory capacitance that interfaces metamaterials with a class of devices known collectively as memory devices.

The ability of metamaterials to create electromagnetic responses absent in nature has initiated the new research field of transformation optics (*1*, *2*), which has applications ranging from electromagnetic cloaking (*3*) to subdiffraction imaging (*4*). Frequency-agile metamaterials, which allow one to adjust the electromagnetic response in real time, are emerging as an important part of this field. The hybrid-metamaterial approach (*5*, *6*), in which natural materials are integrated into the metamaterial composite, has been particularly successful in enabling frequency-agile metamaterials that respond to the application of voltage (*7*, *8*), external electric field (*9*), light (*10*, *11*), and heat (*12*). This tuning ability helps make metamaterial devices more versatile, adapting to shifting input or changing target parameters. However, those methods for enabling frequency-agile metamaterials require the continuous application of an external stimulus to maintain altered metamaterial properties. Once the external stimulus is removed, the metamaterial returns to its original response. Essentially, any functionality derived from metamaterials would benefit greatly if the metamaterial tuning persisted once the triggering stimulus disappeared. Metamaterials that are tuned mechanically or geometrically should retain their tuned properties (*13*, *14*), but such techniques are likely to be difficult to implement at higher frequencies or for complex designs. We have achieved an electrically controlled memory effect using a hybrid device composed of a resonant metamaterial and a transition metal oxide. The principle underlying the persistent tuning of our hybrid device is that of memory-capacitance (memcapacitance for short), which was recently suggested theoretically (*15*).

The persistent frequency tuning of a memory metamaterial device can be illustrated by use of a single-layer gold split-ring resonator (SRR) array patterned (*16*) on a 90-nm-thin film of vanadium dioxide (VO_2) (Fig. 1A). VO_2 is a correlated electron material that exhibits an insulator-to-metal (IMT) phase transition that can be thermally (*17*), electrically (*9*, *18*), or optically (*19*) controlled. The IMT is percolative in nature and is initiated by the formation of nanoscale metallic puddles in the insulating host (*20*). The transition is highly hysteretic and has been previously shown to exhibit memory effects (*21*). The hysteresis associated with the VO_2 can be observed by measuring the dc resistance of the sample (Fig. 1B, solid lines). The phase transition also affects the dielectric properties of VO_2 in a specific way. At the onset of the IMT, electronic correlations acting in concert with the spatial inhomogeneity of VO_2 create a sharply divergent permittivity (*12*, *20*). This increasing VO_2 permittivity increases the capacitance of the SRR resonators so that the metamaterial resonance frequency decreases as the IMT progresses. The data in Fig. 1, B and C, illustrate this effect. At room temperature, we identify the resonance frequency of the SRR array as the spectral minimum at $\omega_0 = 1.65$ THz (Fig. 1C, darkest line). As the dielectric constant of VO_2 is increased with temperature, the resonance frequency red-shifts by as much as 20%. We show that this metamaterial resonance tuning persists when accomplished via short current pulses.

Because both the dc resistance and the permittivity are products of the IMT, the SRR resonance in the hybrid metamaterial inherits the same hysteretic nature observed in the dc resistance (*21*). Any transient excitation that causes a small perturbation in the VO_2 IMT will leave a lasting change of the resonance of the metamaterial. We can apply such an excitation voltage pulse using the electrical leads connected to the device. In this case, the applied voltage promotes the IMT by inducing local heating as current flows through the VO_2 film (*22*). In order to maximize the observable effect that small voltage pulses have on the metamaterial, we adjusted the temperature of the device to a range in which the hysteresis is most pronounced. This corresponds to a range in which the slope of the resistance as a function of temperature, $R(T)$, is the steepest,

[1]Department of Physics, University of California at San Diego (UCSD), La Jolla, CA 92093, USA. [2]Metal-Insulator Transition Lab, Electronics and Telecommunications Research Institute (ETRI), Daejeon 305-350, Republic of Korea. [3]School of Electrical and Engineering, Pukyong National University, Busan 608-739, Republic of Korea. [4]Center for Metamaterials and Integrated Plasmonics and Electrical and Computer Engineering Department, Duke University, Post Office Box 90291, Durham, NC 27708, USA.

*To whom correspondence should be addressed. E-mail: tdriscol@physics.ucsd.edu